arktos (2018) 4:7
https://doi.org/10.1007/s41063-018-0041-3

ORIGINAL ARTICLE

Borehole temperature reconstructions reveal differences in past surface temperature trends for the permafrost in the Laptev Sea region, Russian Arctic

Fabian Kneier[1] · **Pier Paul Overduin**[1] · **Moritz Langer**[1] · **Julia Boike**[1] · **Mikhail N. Grigoriev**[2]

Received: 1 September 2017 / Accepted: 23 March 2018

Abstract
In central Siberia, past temperature changes have been driving permafrost warming in a region with large organic carbon reserves stored in the perennially frozen ground. However, local arctic temperature histories in the ice-rich permafrost areas of the remote Russian Arctic are sparsely known or based on proxy data with potential seasonal biases and underrepresented in circum-Arctic reconstructions. This study employed two inversion schemes (particle swarm optimization and a least-square method) to reconstruct temperature histories for the past 200–300 years in the Laptev Sea region from two permafrost borehole temperature records. These data were evaluated against larger scale reconstructions from the region. Distinct differences between the western Laptev Sea and the Lena Delta sites were recognized, such as a transition to warmer temperatures a century later in the western Laptev Sea as well as a peak in warming 3 decades later. The local permafrost surface temperature history at Sardakh Island in the Lena Delta was reminiscent of the circum-Arctic regional average trends. However, Mamontov Klyk in the western Laptev Sea was consistent to Arctic trends only in the most recent decade and was more similar to northern hemispheric mean trends. Both sites are consistent with a rapid recent warming that is of synoptic scale. Different environmental influences such as synoptic atmospheric circulation and sea ice may be responsible for differences between the sites. The shallow permafrost boreholes provide missing well-resolved short-scale temperature information in the coastal permafrost tundra of the Arctic. As local differences from circum-Arctic reconstructions, such as later warming and higher warming magnitude, were shown to exist in this region, our results provide a basis for local surface temperature record parameterization of climate models, and in particular of permafrost models.

Keywords Temperature reconstruction · Borehole reconstruction · Permafrost · Siberian Arctic · Temperature history · GST

Introduction

Paleoclimate and paleotemperature reconstructions are important tools for assessing the current climatic changes in the context of past variability as well as improving our understanding of interactions in the climate system. By understanding climate responses to conditions in the past, driving processes can be assessed and predictions made for changing conditions in the future. Global and northern hemisphere scale temperature reconstructions illustrate the anomalous character of recent 20th and 21st century warming in the context of the natural variability of the last millennia [9, 16, 23, 45, 57, 63, 67, 72], investigate the cause of warming, supporting anthropogenic over naturally occurring forcing [16, 57], and yield large-scale characteristics of temperature history for the last 2 millennia of up to annual resolution [55, 58, 87] and of millennial-scale resolution for Holocene history and beyond [39, 47, 59]. Based on these centennial-to-millennial-scale records, recent centennial scale warming is a global phenomenon that is most rapid in the north.

Regional studies improve global reconstructions of temperature and reveal spatial deviations from the larger scale

Electronic supplementary material The online version of this article (https://doi.org/10.1007/s41063-018-0041-3) contains supplementary material, which is available to authorized users.

✉ Fabian Kneier
fabian.kneier@awi.de

[1] Alfred Wegener Institute Helmholtz Centre for Polar and Marine Research, Telegrafenberg A45, 14473 Potsdam, Germany

[2] Mel'nikov Permafrost Institute, Siberian Branch, Russian Academy of Sciences, Yakutsk, Russia

Published online: 03 April 2018

mean. In addition, while global scale reconstructions prove useful in assessing the predictions of current large-scale climate models, e.g., their underestimation of the Medieval Warm period [87], regional-scale models might require less spatially averaged temperature parameters. Siberia, in particular, is the site of rapid change, including warming and sea ice loss, but few data that permit temperature reconstructions exist. Briffa et al. [9] find that summer temperatures reconstructed based on tree ring proxies in northern Siberia differed from the global average in that 15th century summers were warmer than summers in the 20th century. Pollack et al. [76] find a similar trend when studying deep borehole reconstructions from three regions in Russia with northeast Siberia exhibiting anomalously warmer temperatures than the other regions in Russia from the 16th to the 19th century. Thus, strong regional or even local differences in past temperature changes may exist in Siberia, but their seasonal (annual, summer, or winter) as well as spatial character remain unknown.

Given that temperature change in the Arctic is 3–4 times more rapid than the global mean [33], there is special interest in the region, but temperature history is sparsely documented. In addition, Arctic climate change may be significantly impacted by internal climate variability. Opel et al. [68] report that regional temperature fluctuations in the last millennium in the Barents and Kara Seas region contain abrupt warming and cooling changes suspected to be connected through sea ice cover to shifting atmospheric circulation patterns. McKay and Kaufman [61] compiled a circum-Arctic paleotemperature reconstruction of the last 2000 years. The compilation's density of records is highest in northeast Canada and Greenland and most sparse in arctic Russia. This uneven spatial coverage gives more weight to western hemisphere temperature changes potentially irrelevant to the thick Pleistocene permafrost of Siberia. In addition, the only Russian proxies included are tree ring data, which are primarily sensitive to summer temperatures and other biological stressors. Meyer et al. [62] have shown that winter paleotemperature trends recorded in ice wedge stable isotopes may not follow summer trends. Poor coverage in the Russian Arctic may also affect Huang et al. [38]'s continental scale reconstructions based on deep boreholes. Again, temperature data are sparsest in Asia and no sources are from arctic Russia.

Understanding past temperatures in central Siberia is important, because organic carbon reserves stored in Pleistocene permafrost are sensitive to temperature changes [84]. Warming and thawing of the permafrost releases frozen organic carbon to degradation, mineralization and release into the atmosphere as greenhouse gas [60]. Although strong regional and local differences in variability in the climate system in the Arctic region have been found to exist, local arctic temperature histories in the ice-rich permafrost areas of the remote Russian Arctic are sparsely known or based on proxy data with potential biases and underrepresented in circum-Arctic reconstructions. Since these local temperature changes have driven past permafrost warming and cooling, they are critical to assessing permafrost interactions with other climate components. In addition, temperature reconstructions from borehole data can provide an independent data set for testing local and regional permafrost model parameterization.

In the absence of trees and multi-decadal ice as provider of proxy data in the arctic tundra, there is a need for other sources to fill the gap between usually longer time scale proxy temperature information from lake sediments such as chironomids, pollen (1 or 2 data points in the last 1000 a [1, 49]) or ice wedge isotopes (centennial resolution and omitting the recent first few centuries due to age control [62]) and direct observational data (if available, reaching back several decades at best). Geothermal reconstructions from permafrost boreholes could help overcome this limitation. While borehole depths of 300 m are estimated to be necessary to reconstruct the temperature of the last 500 a [44], shallower permafrost boreholes present a more frequent albeit not widespread possibility for reconstructions of the last few centuries. For many remote permafrost sites of interest with no observational record, these may yield temperatures of the recent past with relatively good resolution for the first time. In addition, geothermal reconstructions from boreholes respond to the temperature signal throughout the year instead of a seasonal bias.

Our objectives are to (i) reconstruct temperature histories for past few hundred years in our Laptev Sea, Russian Arctic, study region using shallow (100 and 65 m deep) permafrost borehole temperature records and (ii) evaluate our results by comparing them to larger scale reconstructions from this region. In this study, we use two inversion methods (least-square QR and particle swarm optimization) to reconstruct the local ground surface temperature history at two sites: Cape Mamontov Klyk and Sardakh Island, located in the western Laptev Sea and in the Lena River Delta, Russia, respectively.

Study sites and borehole temperatures

The Laptev Sea is located in central arctic Siberia, between the Taimyr Peninsula and the New Siberian Islands (Fig. 1). This region remained unglaciated during the late Pliocene and Pleistocene [22, 83] and is underlain by wide expanses of Ice Complex (Yedoma) deposits of late Pleistocene age on the coastal plains and along large river valleys [31, 83]. Yedoma is composed of ice-rich silts and silty sands with characteristically high organic content (remains of the late Pleistocene mammoth fauna and tundra-steppe flora well

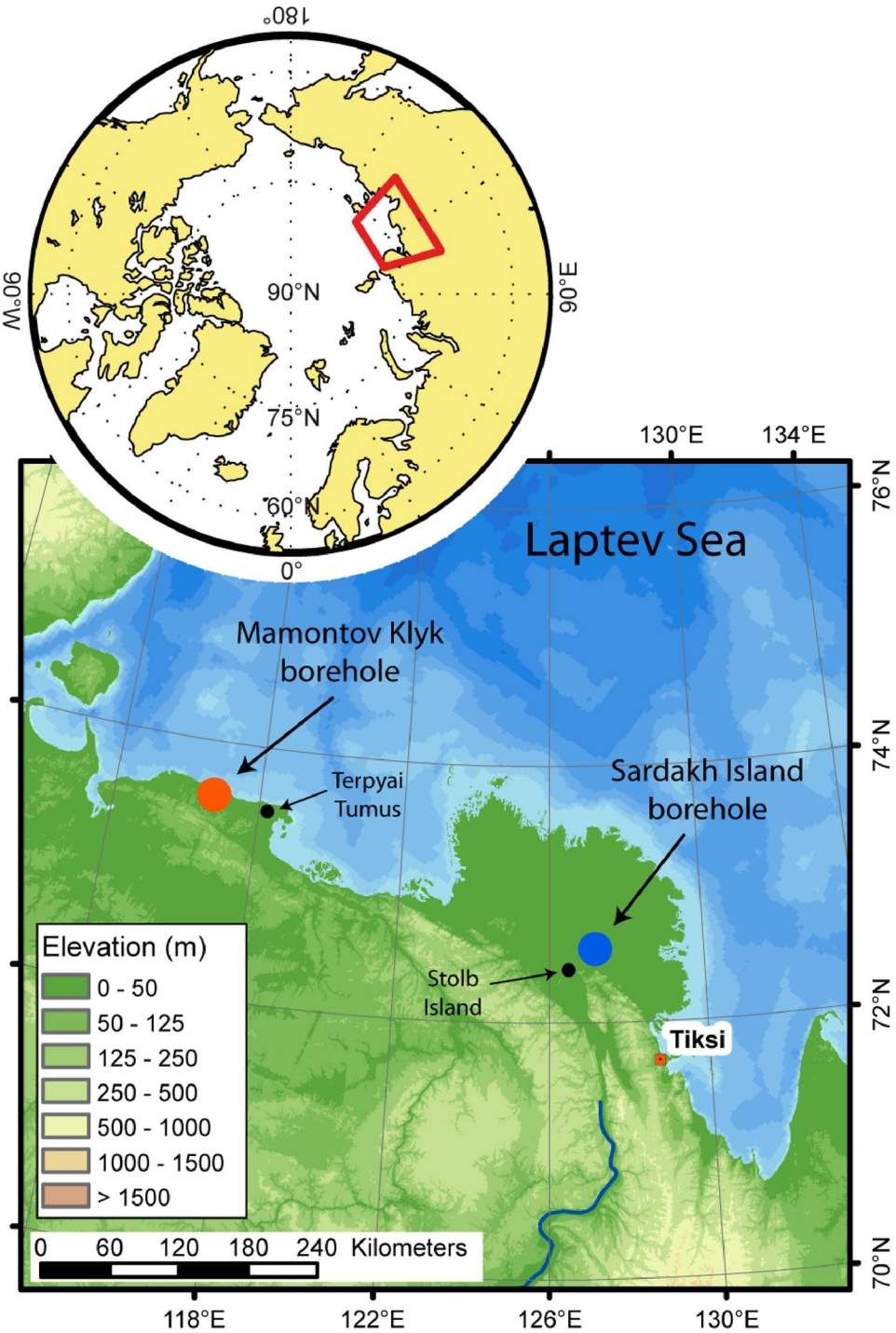

Fig. 1 Western Laptev Sea with the location of the two boreholes: At Cape Mamontov Klyk (65.1 m deep) and on Sardakh Island in the Lena River Delta (100 m deep)

conserved in permafrost conditions) and large penetrating ice wedges. Sedimentation and syngenetic freezing under the late Pleistocene cold–dry-climate conditions created up to 50 m-thick Yedoma deposits [82, 83]. During sea-level low stands, large accumulation plains are considered to have stretched over 200 km offshore of Mamontov Klyk on the continental shelf. Subsequent sea-level rise, inundation, and coastal erosion over the past 11 ka established the present-day shoreline [5]. Due to the continuing long exposure to cold climate, deep permafrost formed. Today, the region lies in the zone of continuous permafrost with thicknesses of 500–1000 m [80].

The general climate in the Laptev Sea region is Arctic continental with 8–9 month winters and short summers of 2–3 months. Winter temperatures are severe, with mean January temperatures of −30 to −32 °C and mean July

temperatures of 3–4 °C [4]. Annual precipitation is between 200 and 300 mm [2]. In winter, cyclones are rare and already in their filling stage. Cloudiness and precipitation are less than in the other arctic regions affected by the Atlantic or Pacific to the east and west. In summer, winds subside and atmospheric circulation weakens. High relative humidity and fogs are common [90].

The Laptev Sea coastal region is part of the northern tundra zone [4, 13]. Active layer thickness in this zone of continuous permafrost is around 30–40 cm [4]. Vegetation is dominated by moss-grass/low-shrub tundra with vascular plants, mosses, and lichens [2].

The borehole locations (Fig. 1) were chosen to represent different subsurface compositions:

Cape Mamontov Klyk lies in the Western Laptev Sea approximately halfway between the Anabar and Olenek Rivers. A 65.1 m-deep onshore core was drilled in April 2005 as part of a coastal and offshore drilling program [71]. The borehole is located on a bluff on the coastal plain where thermokarst and lakes affect about 50% of the coastal plain landscape [30]. The upper stratigraphy of the borehole is Ice Complex deposits of Late Pleistocene origin with ground ice content of up to and exceeding 80% by volume. The subsurface is mostly silty sand with relatively high organic content [81]. The thawing coastal bluff is 25–30 m high, and the coastline currently retreats relatively quickly at 4.5 ma^{-1} compared to an average of 2.5 ma^{-1} for Ice Complex coastlines in this region [28, 97]. In the Western Laptev Sea, upper Cretaceous-Cenozoic sandy-silty deposits several kilometers thick overlie the bedrock. At Cape Mamontov Klyk, at least 2 km of these sandy silts are inferred from seismic–geological profiles [27, 86]. Borehole sediment composition, including organic, mineral, and water contents, is given by Winterfeld et al. [95].

Sardakh Island lies in the southern part of the Lena Delta. A 100 m-deep borehole was drilled in April and May 2009. The Lena Delta has been subdivided into three geomorphological terraces, the oldest of which is exposed in fragments in the southern part of the delta and formed in the middle to late Pleistocene. The second terrace makes up the western part of the delta, a region called Arga Island, and formed in the late Pleistocene to late Holocene, while the eastern terrace is the currently active part of the delta and has been formed since the middle Holocene with shallow modern flood plains [3, 85, 93]. Ice wedge polygons in various stages of development are characteristics of the landscape in the delta [64]. In the central delta, bedrock outcrops are scattered-like islands near the surface. Sardakh Island formed around one of these outcrops [26]. Sediments on Sardakh Island consist of Pliocene and neo-Pleistocene deposits of the southern part of the delta. They are ice-rich deposits of loamy sand and overlie actively deformed layers of sedimentary/carbonate rocks and conglomerates, sand, pebbles, and boulders of Devonian age, indicating intensive pre-Pliocene reworking [25]. These can contain lithified organic material and even large pieces of lithified wood [24, 26]. Bedrock may lie close to the surface as suggested by gravity data [48], but its depth below the surface is unknown. Sardakh Island is undergoing current neotectonic uplift [27] and its elevation of currently about 40 m is comparable to the oldest terrace (though different in genesis). The island's surface is characterized by ice wedge polygons of presumably late Pleistocene origin [25] and a few thermokarst lakes of 30–500 m in diameter.

In contrast to Mamontov Klyk, meteorological data are available from the southern Lena delta: Wagner et al. [93] report mean annual air temperature of −14.7 °C and mean annual precipitation of 190 mm. The 9 month winter with average and minimum temperatures of −30 and −48 °C, respectively, brings heavy snowstorms, while the summer period has average and maximum temperatures of 7 and 18 °C [93]. Recently, Boike et al. [7] report slightly warmer annual mean air temperatures of −12.5 °C from 1998 to 2011.

Both boreholes are part of the Global Terrestrial Network for Permafrost (GTN-P). At both sites, thermistor chains were installed, recording at 1 h interval (Mamontov Klyk) and 6 h interval (Sardakh). Mean temperature profiles for the last year of available data from both boreholes are presented in Table 1. They are used as the target temperature profiles in the temperature reconstructions. We discard the top measurement, which lies in the active layer. Removing top measurement depths potentially influences the most recent time in the reconstruction. The effect here, however, is negligible, as even the annual temperature signal penetrates much deeper than these missing target depths.

The deepest temperatures recorded by the logger chain at Sardakh Island varied annually by about 0.05 °C, although they were below the damping depth for annual surface signals. These variations were probably a result of cooling and warming of the data logger at the surface. Therefore, only longer than annual trends are regarded when using sensor time series data below 20 m.

Inversion method

To estimate temperatures at times prior to the start of direct observation, the diffusive slow transfer of heat into the ground to different depths on different time scales can be taken into account, and a surface temperature history can be reconstructed that is consistent with the observed temperature profile in the borehole. In this study, we use an adaption of two inversion methods previously applied to temperature measurements from ice core sites [78].

Table 1 Mean temperature of observed borehole profiles from 14.08.2010 to 13.08.2012 (Mamontov Klyk) and 23.08.2011 to 22.08.2012 (Sardakh Island)

Mamontov Klyk		Sardakh Island	
depth (m)	Mean Temperature (°C)	depth (m)	Mean Temperature (°C)
0.1	− 9.36	0	− 8.68
1.1	− 9.34	0.4	− 8.66
2.1	− 9.63	0.8	− 8.71
3.1	− 9.78	1.2	− 8.80
4.1	− 10.04	1.6	− 8.93
5.1	− 10.26	2	− 8.91
6.1	− 10.50	2.5	− 9.04
8.1	− 10.84	3	− 9.14
12.1	− 11.37	4	− 9.24
14.1	− 11.57	5	− 9.36
16.1	− 11.71	7	− 9.58
18.1	− 11.85	9	− 9.73
20.1	− 11.93	11	− 9.86
22.1	− 12.08	13	− 10.02
30.1	− 12.21	15	− 10.11
35.1	− 12.29	20	− 10.33
40.1	− 12.43	30	− 10.56
45.1	− 12.50	40	− 10.59
50.1	− 12.54	50	− 10.52
55.1	− 12.53	60	− 10.53
60.1	− 12.54	70	− 10.38
65.1	− 12.54	80	− 10.24
		90	− 10.20
		100	− 10.19

The inversion scheme employed a flux-conserving finite volume numerical soil model for heat conduction in the subsurface. This forward model was used to calculate temperature vs. depth profiles from surface temperature histories. The inversion schemes optimized temperature history in a least-square sense: they minimize the deviation of the forward model output from the observed temperature profile in the borehole, i.e., the unweighted root-mean-square (RMS) error:

$$E_{\mathrm{rms}} = \left(\frac{\sum_{i=2}^{i_{\max}} \left(T_{\mathrm{model}}(i) - T_{\mathrm{obs}}(i) \right)^2}{i_{\max} - 1} \right)^{0.5} \quad (1)$$

to yield a best fit solution for the surface temperature history, where T_{model} is the modelled temperature distribution and T_{obs} the observed temperature data, as shown in Table 1.

Forward soil model

Diffusive heat transfer is solved numerically in a one-dimensional flux-conserving finite volume scheme (Eq. 2). Freeze-thaw processes are considered in a three-phase heat capacity/conductivity model based on de Vries [92] and modified following Ippisch [42] to incorporate the phase change between water and ice (Eq. 3):

$$c_{\mathrm{eff}} \times \frac{\partial T}{\partial t} = \frac{\partial}{\partial z} \left(\lambda \times \frac{\partial T}{\partial z} \right) \quad (2)$$

$$c_{\mathrm{eff}} = \sum_i c_i \theta_i + L_f \frac{\partial \theta_w}{\partial T}, \quad (3)$$

where c is heat capacity, θ_i volumetric fraction of phase i (mineral, water, and ice), L_f latent heat of freezing, and λ thermal conductivity.

Subsurface thermal properties were retrieved from either the observed temperature field or the sediment composition analysis of the borehole (ESM.2).

Initial and boundary conditions

The time varying upper boundary temperature corresponded to the temperature history. The lower boundary condition was set to the geothermal flux of $Q = 53$ mW/m^2 [41, 75]. The one-dimensional soil model was solved as a mixed boundary-value problem with the upper boundary being forced by the external temperature variable itself (Dirichlet boundary condition), while the lower boundary was specified by the thermal gradient (Neumann boundary condition) [40].

The heat stored in the subsurface could be underestimated if the bottom boundary condition placement (BBCP) was too shallow and perturbs the subsurface temperature field [89]. Based on Smerdon and Stieglitz [88], we identified the necessary BBCP in our model to be at least 550 m below the borehole to prevent boundary condition-related amplitude attenuation within the borehole. We placed the bottom boundary condition well below this threshold at 1000 m.

The initial temperature profile was constructed using temperature observations from a 500 m-deep borehole near Tiksi [29]. Extrapolation below was done by extending the constant heat flux, taking into account the change in temperature profile slope below the permafrost for saturated sand conditions at Mamontov Klyk. Due to its rocky subsurface with low water content at depth, there was no such distinct change in the slope at Sardakh Island. The whole profile was shifted to match the bottom temperature at each site by adding a constant offset. Linear approximation from 20 m

upwards to the surface was accommodated dynamically in the optimization process using the initial value of the currently valid surface temperature history.

The model implicitly assumes that (i) advective heat transport is negligible, (ii) there are no internal heat sinks or sources in the sediment, (iii) frost heave and the effect of volume changes associated with the phase transition of water and ice are neglected, and (iv) that there is no lateral heat flux.

Optimization

The inversion problem of surface temperature reconstruction does not have a unique solution due to the diffusive nature of heat transport. A heat pulse at the surface spreads spatially as it diffuses into the ground. Temperature at one specific depth, therefore, contains contributions of surface temperature from a range of past times. As a result, an infinite number of possible temperature histories can fit the observed temperature profile perfectly [15] and the problem is underdetermined. The resolution power of borehole temperature reconstruction is limited by this diffusive spreading, which effectively smooths out extrema over time. The result is that the recovered temperature for a certain year in the past is effectively the weighted average of the temperatures in a range around that year. The width of that range grows larger with increasing time into the past [70]. Using theoretical calculations in a homogeneous subsurface, Demezhko and Shchapov [19] estimate the minimum event length resolved in the current ground temperature field to be $\pm 1/3 \times t'$ around the time t' before the borehole observation. Consequently, we choose methods that do not specify high-frequency changes in the past. In addition, a procedure of averaging with non-uniform running windows should be used whenever comparing temperature time series of constant temporal resolution (such as annual observations) to geothermal reconstructions [18]. To estimate the past surface temperature history T_j from the borehole temperature observations, two inverse methods (LSQR and Particle Swarm) were used with the forward soil model to optimize a surface temperature history for each of the borehole sites (Sects. "Least-squares method (LSQR)" and "Particle swarm optimization (PSO) method"). To estimate the time period for which information can be reconstructed from the borehole temperatures, the characteristic penetration depths of thermal heat waves were analysed using the forward model for the two sites (Sect. "Optimization").

Least-squares method (LSQR)

The least-squares QR (LSQR) inversion [78] is a generalized least-squares method (see ESM.3 for more details). Its outcome is a single best solution with minimal variance, that is, the updates on the history to minimize E_{rms} are distributed as evenly over the time span as a locally linearized response allows. To take into account the resolution power discussed above and that only longer wavelength heat waves penetrate to deeper depths with significant magnitudes, for that response, the surface temperature is varied over a minimum event duration [19] around each year. The initial choice of surface temperature history was a linear interpolation of the observed temperature profile vs. depth mapped linearly to the reconstructed time domain.

Particle swarm optimization (PSO) method

In particle swarm optimization (PSO), a group (= swarm) of particles searches in the space of all possible temperature histories to find the best fit to the observed borehole temperature profile. The space of all possible histories is parameterized and the coordinates of a point in the space represent a temperature history. A group is randomly initialized with positions in the search space as well as with velocities with associated inertia keeping the particles on their current trajectories. Each particle evaluates its current position's temperature history and RMS error using the soil forward model. An iterative update to each particles velocity is given by an attractive component drawing a particle in the direction of the position of the best fit so far evaluated by any swarm member, and determines the new position for the next iteration. Due to the combination of attraction and inertia, the method leads to a broad exploration of the search space while focussing specifically on regions with good overall match (RMS error) to the observation. The search terminates once a temperature history with E_{rms} below a specified input threshold is encountered. Many runs with different random initializations were performed and the resulting best fits analysed statistically. This swarm optimization approach is well suited to the nonlinear diffusive character of the problem and a large dimensional search space with potential multiple local and global minima. We used a Matlab implementation of the PSO method by Ebbesen et al. [21].

Table 2 Input optimization parameters for the particle swarm implementations

Optimization parameters	
Swarm size	30
Maximum generations	400
Attraction towards personal best	0.5
Attraction towards global best	3
Limit of velocity of particles	Limited to 10% of the parameter range.
Range of random initial positions	−16.2 to −10.2 °C

Systematic variation of the optimization parameters in the implementation resulted in values given in Table 2 to yield most robust search results, i.e., the probability of a single swarm reaching the specified input E_{rms} threshold. Paleotemperature reconstructions for the northern hemisphere and for the Arctic predict anomalies on the order of < 1 and 1–2 °C over the last 2000 years, respectively [58, 61]. For the initial random particle positions, a subspace of three times the larger Arctic range around the Tiksi air temperature average of 1961–1990 was chosen (Table 2).

To inhibit unresolved high-frequency variations, two choices of parameterizing the search space of possible temperature histories were applied:

Four-segment PSO The four-segment parameterization applied by Roberts et al. [78] in his ice borehole reconstructions. The temperature histories were simplified to four consecutive linear ramps with transition points that were variable during optimization. In this eight-dimensional parameterization, the variables to be optimized are the time and temperature of the three transition points as well as the temperature of the start and end.

Fix time point PSO Fixed time points were spaced, such that the span of ±1/3 around them did not overlap adjacent spans. In this parameterization of the search space, only the temperatures at each fix time point varied. The advantage was effectively a higher number of segments which should be more stable at higher search space dimensionality in the optimization as changes are fully independent of each other, which was not the case as fully in the four-segment parameterization (changing the location in time of an intermediate point simultaneously affects the temperature at the old point). A disadvantage is that temporal resolution is a priori limited even if the temperature observations could offer more information. In addition, the resulting temperature history curve appears less smooth, because past temperatures are optimized at discrete time ranges.

For both (four-segment and fix time point), 500 stochastic runs of the swarm optimization with random swarm initializations yielded a population of temperature histories. The median was selected as the most likely temperature history and the variation about the median indicate uncertainty including potential short-term variations that are smoothed out by diffusion.

In contrast to the LSQR method, the PSO method employs a Monte Carlo approach to explore the range of possible solutions. Its outcome is a distribution of possible solutions with the freedom of producing sharper changes than the LSQR method. Therefore, we expect the LSQR method to smooth out sharper changes more than the PSO method.

Results

Optimization

The conservatively adopted maximum recoverable period for the borehole depths was 225 a for the Mamontov Klyk borehole site and 260 a at the Sardakh Island borehole site using characteristic penetration depths in homogeneous subsurface conditions and performing LSQR calculations to deal with the limitations of heterogeneous layering at Sardakh (ESM.4). The LSQR implementation was run calculating updates to improve the E_{rms} and saving the result in 0.01 °C steps of decreasing E_{rms}. The lowest attained limit was 0.04 °C at both sites. The distribution of temperatures in the PSO inversion achieved an E_{rms} in the median solution for the fix time points PSO of 2.77×10^{-2} and 2.66×10^{-2} °C, for Mamontov Klyk and Sardakh Island, respectively. In this respect, the four-segment-parameterized PSO inversion fell short of both the LSQR and the fixed time point PSO (5.46×10^{-2} and 4.28×10^{-2} °C at the two sites, respectively) (See ESM.5). The resulting optimal temperature histories are shown in Fig. 2.

Surface temperature reconstructions

For the Mamontov Klyk site, the LSQR solution shows almost constant temperature levels of −14.2 °C starting before 1800 and continuing throughout the 19th century with only a small one tenth of a degree Celsius rise between 1860 and 1873. A gradual transition to rising temperatures begins in the first decade of the 20th century and warming increasingly in the second half of the century. A slowing of the warming occurs in the 1990s and a maximum of −11.5 °C is reached in 2002. A slight cooling of 0.4 °C follows until 2004 when a recent final strong linear increase sets in culminating the temperature history at −9 °C in 2011, the time of borehole logging. The median solution from the fix time points PSO exhibits a generally similar pattern with gradual deviations. Temperatures start around −14 °C before 1800 falling slightly but gradually by 0.25 °C per century throughout the 19th century before beginning to warm as well in the first decade of the 1900s. The warming rate, however, remains lower with temperatures up to c. 0.3 °C below the LSQR curve, the rate increasing only later in 1950 and again in the 1970s. The PSO shows warming eventually superseding the LSQR level and reaching a maximum 0.6 °C warmer around the same time (2003). The magnitude of the subsequent cooling is double the LSQR value and the cooling period lasts twice as long. The final increase occurs in the last 2 instead of 5 years. This solution thus shows the sharpest

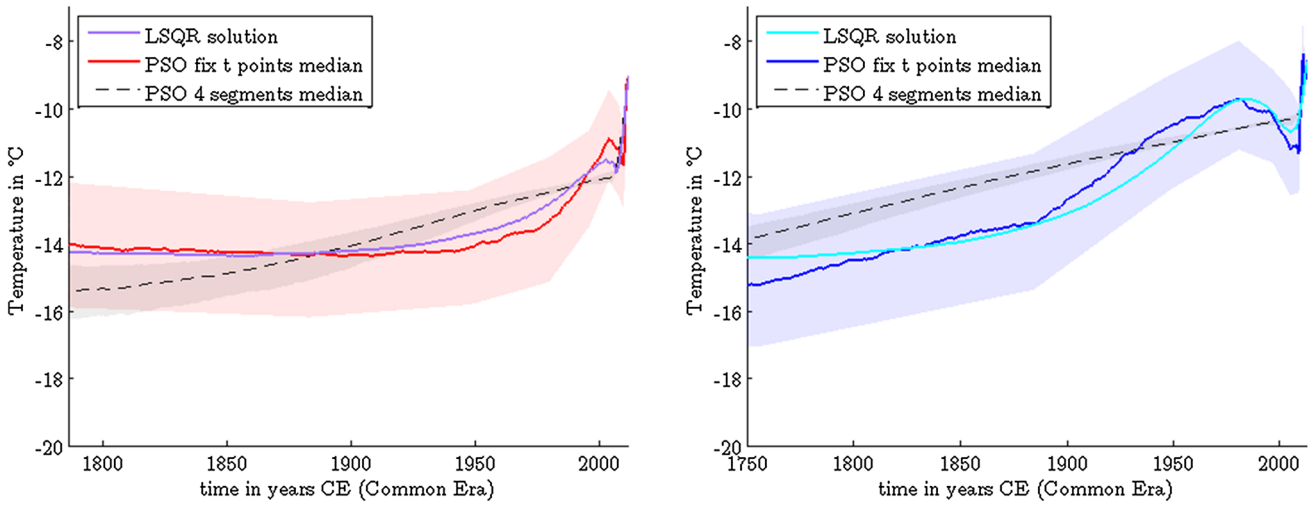

Fig. 2 Reconstructed ground surface temperature history (left) at Mamontov Klyk and (right) at Sardakh Island using the LSQR and both PSO inversion methods. The shaded area gives the 25th and 75th percentile in the PSO distribution

final increase of the three reconstruction methods. The four-segment PSO solution stands apart from the two other solutions. It matches the feature of the recent temperature rise but appears to instead almost linearly decrease backwards prior to that going straight through the variations of the other two curves from 1800 to c. 1980, warming rather steadily by 3 °C in two centuries.

For the Sardakh Island site, the LSQR solution shows almost constant temperature levels of −14.3 °C during the 18th centuries with variations of only one 10th of a degree Celsius. A gradual warming begins in the course of the 19th century, significantly increasing in its rate after the turn to the 20th century. Temperatures rise continuously to a maximum of −9.7 °C in the 1980s. The solution displays a subsequent pronounced drop of 1 °C until 2004 before commencing a final large increase in recent years to a maximum of −8.6 °C in 2012, the time of borehole logging. The median solution from the fix time points PSO is made up of coarser ramp periods than the LSQR solution, especially recognizably in the further past. Nonetheless, its solution again exhibits a similar pattern with a few notable deviations. Temperatures begin at a minimum of −15.2 °C in the middle of the 18th century. Temperatures recover by 1.4 °C per century until the end of the 19th century when a further increase in the warming rate to 4.6 °C per century is evident until 1950. This warming continues to a maximum temperature of the same level as in the LSQR but attained slightly earlier in 1979. The subsequent cooling is broken into two consecutive steps, but the magnitude of the overall drop is again over one-and-a-half times as large as in the LSQR falling as low as −11.3 °C. As the solution reaches the same final temperature, the last increase to −8.6 °C is even larger, 2.7 °C in 4 years. The four-segment PSO solution coincides only in the most recent sharp temperature increase, but shows a differing behavior before that point. It is characterized by an almost linear decrease backwards with −1.4 °C per century cutting through the troughs and peaks of the other two curves.

Figure 3 presents the temperature profiles down the Mamontov Klyk and Sardakh Island boreholes from observation and by the forward soil model for the inversion solutions of all three methods. In general, forward modelled borehole temperatures from the LSQR and fix time point PSO solutions agree with the observation and with each other (Fig. 2) to within sensor accuracy. Borehole temperatures calculated from the four-segment PSO solution have the poorest agreement with temperature observations around a warmer excursion at 30 and 35 m depth for Mamontov Klyk and a similar excursion at 50 m and a temperature overestimation at 20 m depth for Sardakh Island, though, due to poorer sensor accuracy at Sardakh, even the four-segment PSO profile lies within the uncertainty range. At Mamontov Klyk with its better sensor accuracy, four-segment PSO clearly does not agree to within observation uncertainty. Agreement to these features of the observational record in the reconstruction solutions of the other two methods was also only observed at the final lower E_{rms} thresholds, indicating that such agreement is connected with the ability to achieve lower E_{rms} limits than obtainable with the four-segment PSO inversion.

Thus, the LSQR and the fix time points PSO inversion solutions agree quite well with each other (to an RMS deviation between the two histories of 0.27 and 0.40 °C, at Mamontov Klyk and Sardakh, respectively) and with the observation (to an E_{rms} of less than 0.03 °C and maximal errors of 0.05/0.06 °C in forward modelled temperature) at

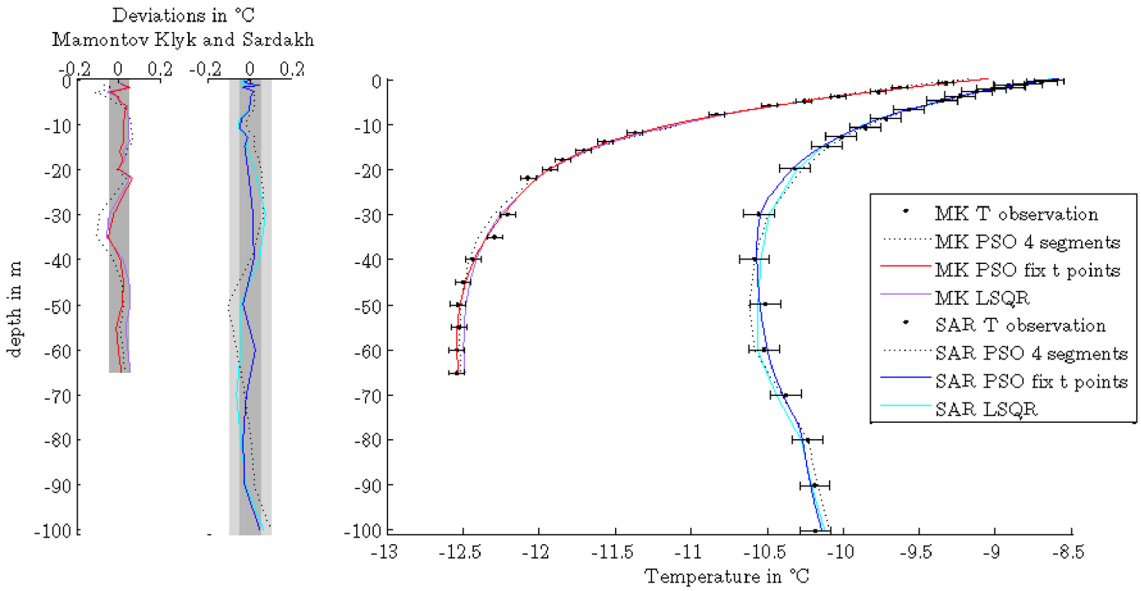

Fig. 3 (Right) The temperature profiles down the two borehole sites from observation and by the forward soil model for the LSQR and both PSO median surface temperature reconstructions. Thermistor accuracy was 0.05 °C at Mamontov Klyk but only 0.1 °C at Sardakh Island. (Left) Deviations from observed profiles for both sites. The dark grey area represents 0.05 °C deviation and the light grey area represents the larger uncertainty at Sardakh

both sites. The four-segment PSO reconstruction shows a generally differing temperature history (a three times higher RMS deviation to the other two solutions) and forward modelling yields a smoother temperature profile that captures variations in the borehole profile less well. This method is not able to resolve the temperature variations over the relatively long recoverable time period of modelling (ESM.8).

For a comparison of the ground surface temperature histories of Mamontov Klyk and Sardakh Island, we considered the temperature histories given by the optimal inversion solutions of the LSQR and the fix time points PSO. Solutions at both sites showed a similar warming trend from the colder temperatures of the previous centuries, followed by a maximum and cooling in recent times and a sharp final increase in temperature during the last half decade before 2011/2012. They differed, however, in the timing of the warming as well as the magnitude of the first warming and subsequent cooling in recent times. At the start of the reconstruction, both exhibited almost constant temperatures with variations of only a tenth of a degree and temperature levels are of similar magnitude of c. −14.2 °C (Mamontov Klyk) and −14.3 °C (Sardakh). Temperatures at Sardakh began to rise around 1850 and continued to a maximum of about −9.6 °C at the start of the 1980s. This was followed by a pronounced cooling by 1–1.6 °C over the 13 years before 2004. At Mamontov Klyk, on the other hand, the transition to warmer temperatures commenced almost a century later and rose to a maximum of only -11.5 to −11 °C in the first decade of the 21st century, 3 decades later than Sardakh. The subsequent cooling was also less (0.4–0.8 °C) and lasted only for half a decade. The final strong increase in temperatures began only between 2006 and 2009, when it rose to −9 °C in just 2 years. In contrast, this most recent temperature increase commenced earlier at Sardakh (between 2004 and 2008). In addition, although prior maximum temperature levels here had been higher, due to its previous more pronounced cooling, the overall temperature change to the 2011/2012 maximum of −8.6 °C was almost the same as at Mamontov Klyk (2.1–2.8 °C vs. 2.6–2.9 °C). The final (2011 at Mamontov Klyk, 2012 at Sardakh Island) ground temperatures at both sites were almost similar (−9 vs. −8.6 °C).

Discussion

Comparison to other temperature data

Figure 4 shows the trends of the resulting temperature histories at Mamontov Klyk and Sardakh Island in comparison to other local records from the region as well as to larger scale temperature trends. To be able to compare these records to the geothermal reconstruction, their annually resolved time series were averaged using the non-uniform running windows of the minimum event resolution referenced to the year 2011/2012 CE [18].

For the most recent time span, the results can be compared with direct observational data. The longest record of surface air temperature in the region is available from Tiksi

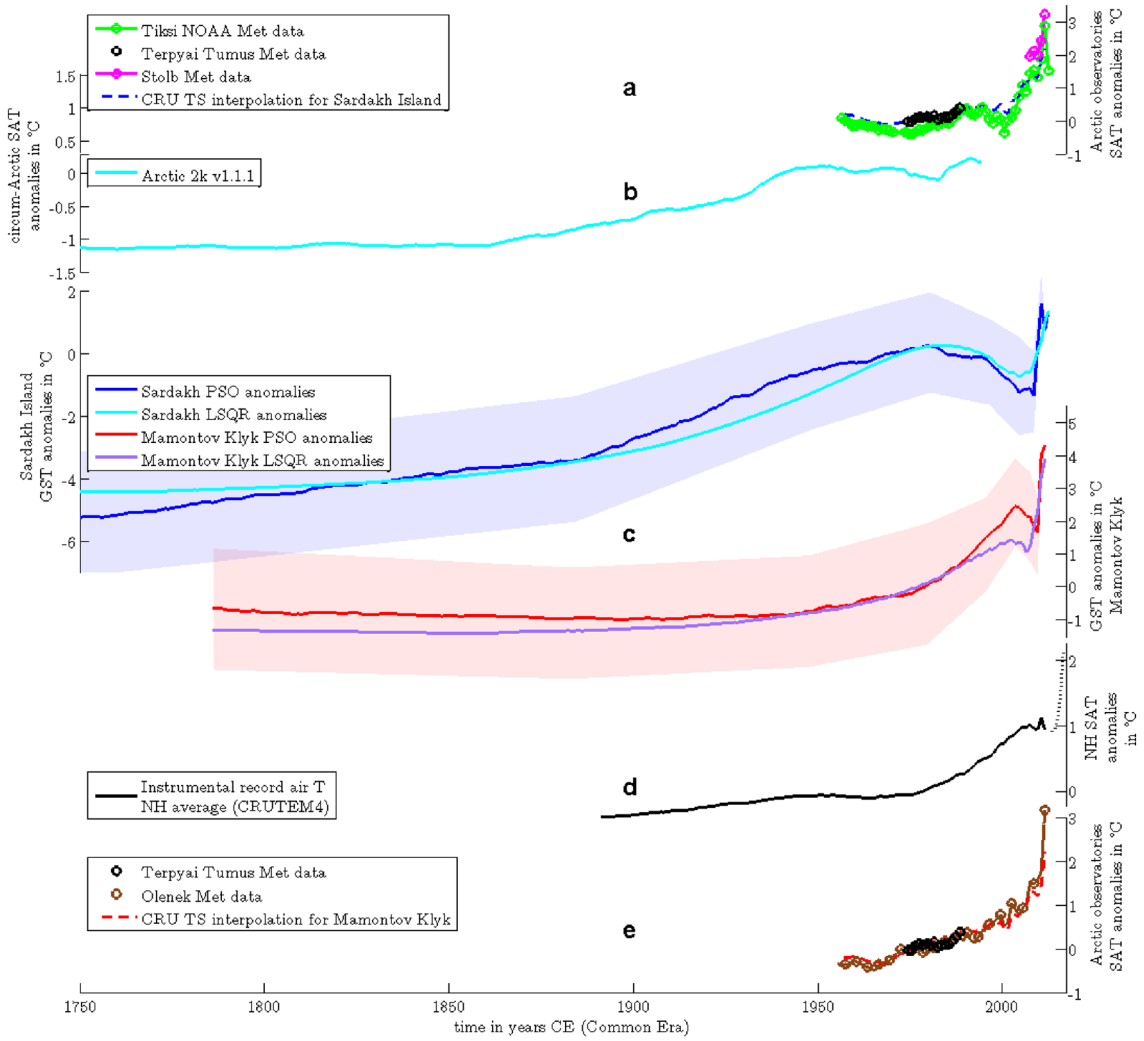

Fig. 4 a, e Regional surface air temperature (SAT) anomalies at Tiksi [65], Terpyai Tumus [11], Stolb Island [77], Olenek (68.5°N, 112.43°E) [54], and the CRU TS grid interpolation [34] for Sardakh Island and Mamontov Klyk. **b, d** Two longer scale records, (light blue) circum-Arctic proxy-based temperature compilation from PAGES 2k Consortium [72], and (black) the northern hemispheric mean temperature anomalies of the instrumental record [46]. **c** Anomalies of the two reconstructed ground surface temperature (GST) histories at Mamontov Klyk (red) and Sardakh Island (blue) from the LSQR and fix time point PSO inversions. The Terpyai Tumus record is shown twice, in comparison to the Tiksi trend and the Olenek/Mamontov Klyk CRU TS trend. All anomalies are referenced to the 1961–1990 period where possible. The averaging process shortens the record lengths from the periods given in the text. Note the factor of 2 in the scale of the hemispheric and circum-Arctic larger spatial averages

(1930s to present), a shorter period record (1961–1996) from Cape Terpyai Tumus in the vicinity of Mamontov Klyk, and a short recent record from Stolb Island in the Lena Delta (2005–present). Of these, only the 60 a of observational data from Tiksi are long enough to indicate a trend. The observational period from Terpyai Tumus is enough to calculate the climatic 1961–1990 average, but the period is too short to clearly distinguish trends. The few years' record at Stolb did not allow for a 1961–1990 reference determination, but employing the Tiksi reference (located 118 km to the southeast) to calculate anomalies, they appear to match the Tiksi trend well, indicating that there is good agreement between these (relatively nearby) stations. Similarities can be seen to the reconstructed temperature history at Sardakh Island in the magnitude of the recent increase by 3 °C and in the earlier timing of the onset of the increase already in 2000. The higher temperatures in the middle of the 20th century in the Tiksi record also agree with the reconstructed Sardakh trend while contrasting the trend of lower temperatures at Mamontov Klyk.

A longer observational data set from 1850 CE onward is given by the spatially averaged northern hemispheric instrumental record of land air anomalies compiled by the Climate Research Unit of the University of East Anglia [46]. On this

larger scale average, temperatures increase only slightly until the middle of the 20th century, after which significant continuous warming sets in. A plateau and slight cooling occur only in the first decade of the 21st century. These periods are reminiscent of the reconstructed Mamontov Klyk temperature trends albeit a factor of 2 lower in magnitude. However, while the Mamontov Klyk reconstruction began increasing again by 2011, the instrumental record shows a comparably rapid recent increase only in the four years up to 2016, following the borehole record (dotted line in Figure). Mamontov Klyk is undergoing recent surface temperature increases that are ahead of the hemispheric trend but consistent with the Arctic synoptic trend. Olenek, a station located 500 km south of Mamontov Klyk (68.5°N, 112.43°E), exhibits a similar trend of a steady increase from the 1930s onward and with relatively low temperatures in the middle of the century.

For periods prior to the availability of direct observations, our temperature reconstructions can be compared to other borehole temperature or proxy-based climate reconstructions. Our 3–4 °C variation between 1900 and 2000 is within the range of other arctic site measurements. Lachenbruch and Marshall [50] demonstrate that Alaskan permafrost subsurface temperatures indicate a spatially variable but widespread warming of the permafrost surface of 2–4 °C during the previous few decades to century. Subsurface borehole temperature reconstructions on a northern hemispheric scale show an increase of 0.9 °C from 1750 to 2000 [37, 38, 74]. Given that Arctic warming is amplified and 3–4 times more rapid than the global mean [33], our reconstruction's increase of 2.7 °C at Mamontov Klyk until 2000 and a 3.9 °C increase at Sardakh in the same period are reasonable. The variation at Sardakh within this period is, however, even higher with a maximum of 5 °C, placing it at the higher end of expected temperature change. A regional circum-Arctic proxy-based reconstruction with potential bias to western hemispheric influences is given by McKay and Kaufman [61] for the period of 1–2000 CE (Arctic2k). This record overlaps the time span of the Tiksi observational record from 1956–1994. The Arctic2k and Tiksi anomalies have similar trends, but the Arctic2k varies less (by more than a factor of 2) than Tiksi, so that the larger scale mean is again more moderate than our local record. Nonetheless, both records indicate a warmer period beginning in the 1980s, a minimum in 1960, and warmer temperatures prior to that minimum. Therefore, we suggest that the Tiksi record follows the circum-Arctic trend and furthermore that this region indicates temperature changes amplified over even the Arctic mean. Mean Arctic temperatures show warming from the 1850s onwards, reaching their warmest pre-2000 levels from the 1940s on. Together with the fit to the recent Tiksi record, these trends are similar to the reconstructed Sardakh Island temperature trends. Both begin to rise around 1850, a century ahead of such warming at Mamontov Klyk, both show elevated temperatures between 1931 and 2000, and a similar recent rise of 2.7–3 °C.

Despite their similarities, the reconstructed histories in the Laptev Sea region at Mamontov Klyk and Sardakh Island suggest some local differences in permafrost surface temperature history. While Sardakh Island is more similar to regional Arctic temperature trends, Mamontov Klyk is consistent with Arctic trends only in the most recent decade and is more similar to northern hemispheric scale mean trends before then. There is consistency between our Sardakh reconstruction and observational records from Tiksi and Stolb. The only record from the vicinity of the Mamontov Klyk borehole is from Terpyai Tumus. This record is only 30 years and not long enough to correlate it with either reconstruction, but there is consistency between our Mamontov Klyk reconstruction and a record from Olenek (Fig. 4) albeit the latter being further south. In addition, consistency is indicated between our reconstructions and temperature data from the CRU TS grid, interpolating instrumental observations to the remote locations of Mamontov Klyk and Sardakh Island, with agreement to the two differing trend types, respectively.

Despite the differences between both borehole reconstructions, it is interesting to note that the final ground temperatures (2011 and 2012) at both sites were almost similar. The reconstructions' ground surface temperatures for both sites were also almost equal two centuries ago, i.e., levels of −14.2 and −14.3 °C, although the assumed climate as well as the deeper permafrost temperatures observed in the boreholes suggest a colder climate at Mamontov Klyk. This might indicate colder initial ground temperatures at Mamontov Klyk well before the time period reconstructed in this study.

Site differences

Reasons for the differences in the reconstruction between the two sites could be differences in environmental influences. The two borehole sites are about 350 km apart and differ in meteorology, atmospheric circulation including impact from snow cover, long-wave radiation, geothermal heat flux, sea ice, and river heat, which may influence their ground surface temperature history.

Mamontov Klyk is far from major river influences but directly at the coast of the Laptev Sea. Sea ice formation and its effect on climate might have a direct influence on the prevalent temperature history [43] and rapid sea ice loss has been connected with accelerated Arctic land warming [53]. Changes to advected heat will thus be sensitive to changes in sea ice cover or open water season duration and to surface water temperature changes. Both changes are difficult to quantify but consistent with warming over the past half century. In the central Laptev Sea,

open water season has been reported to have increased by 15 days per year on average for the 2010–2012 period from the previous 20 year mean [32].

In contrast, Sardakh Island is located in the middle of a large delta. It is separated from the open ocean and its influences by more than 75 km of intervening deltaic deposits, lakes, and river channels. It is adjacent to a major discharge channel of the Lena river which transports heat several hundred kilometers (year-round, in winter under up to 1.5 m river ice) from warmer southerly latitudes. Observational records suggest that both discharge [73] and heat transport [96] are increasing. Additional lateral heat input could dominate over the surface temperature forcing if (i) a strong enough temperature difference between river and surface temperature exists over long time periods or during a sensitive season, e.g., warm river forcing could prevent winter cooling of the ground, altering the annual mean temperature to a more moderate magnitude than the meteorological trend would predict and (ii) the heat flux from the river at the borehole location is of comparable magnitude to the surface heat flux. To better understand the influence of the Lena River as a local heat source, observations of heat flux in the river bed and banks adjacent to the borehole would provide an indication of the temperature perturbation at the borehole, and support numerical modelling of heat conduction. In general, though, we do not expect the river influence to strongly dominate due to the good agreement with SAT trends of the closest observatories in Tiksi and Stolb.

The trends of environmental changes at both Mamontov Klyk and Sardakh are consistent with reconstructed temperature records. Differences between their dominating environmental influences may be responsible for differences between the sites.

As part of the atmospheric circulation patterns, cloudiness during winter is another factor influencing the surface temperatures. In the surface energy balance, net radiation during the winter period is mainly determined by the long-wave radiation, with increased cloudiness leading to decreased outgoing long-wave radiation and warmer surface temperatures. Changes to cloudiness, i.e., the evolution of winter time cyclone activity at the sites, could drive the evolution of permafrost temperatures [51], but are difficult to assess. Vavrus et al. [91] show increased autumn cloudiness associated with recent sea ice minima and further suggest that the rapidly declining Arctic sea ice will be accentuated by changes in polar clouds. The differences between the sites might indicate general differences in atmospheric circulation with cloud cover such as cyclonic activity.

Although geothermal heat flux has been shown to vary over very short spatial scales, e.g., in Antarctica by over 150% over 10–100 km [12], the global map of heat flux in Davies [17] gives values that differ only by less than 5% between the sites.

Differences could potentially originate from snow cover impact and its influence on differences between ground and air temperatures. If long-term snow cover variation differed spatially between the two sites, the same air temperature history could yield differences in the ground temperature history. Langer et al. [52] report that 10 mm deviation in snow water equivalent could translate to up to 2.5 °C deviation in ground temperatures at 2.5 m depth on annual to decadal time scale. No long-term snow cover observations exist for either site. However, interannual variations of snow depth analysis data from the Canadian Meteorological Centre (CMC) for the period of 1998–2015 [10] appear to be correlated (Fig. 5), suggesting that both sites are similarly affected by synoptic variations during this time period. During the data period, Mamontov Klyk exhibits a generally higher mean snow cover (10 vs. 7 cm) with only a few exceptions where severe winters at Sardakh lead to thicker snow cover relative to Mamontov Klyk (winter of 1998/99, 2005/6, 2008/9). Regarding the annual mean trend in snow depths, a general similar pattern at both sites is apparent. At decadal-to-centennial time scales, other borehole studies [6, 14, 35] (see ESM.1) indicate air-ground coupling even with changes to snow cover and soil moisture.

Methodological considerations

In the geothermal method used, the borehole temperature profiles have a direct association with temperature in the ground surface temperature (GST) history (since they are the direct physical remnants of past changes at the surface). This direct relationship removes ambiguity related to the necessary calibration introduced in proxy record reconstructions, which affects temperature inference [36]. The disadvantage in geothermal reconstructions, however, is a progressively

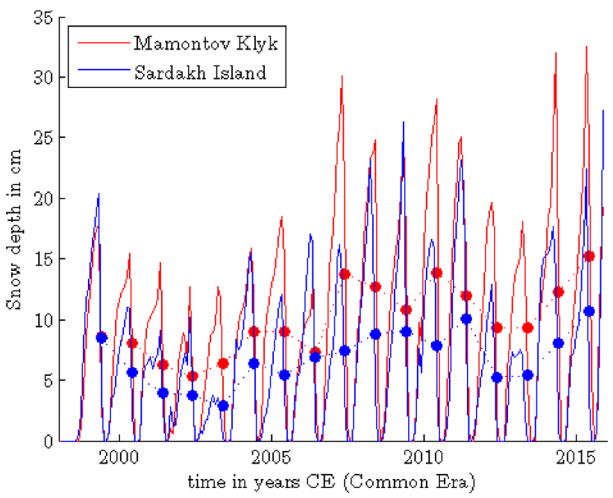

Fig. 5 Monthly snow depth analysis data [10] for the Mamontov Klyk and Sardakh Island locations. Dots represent the annual mean

lower resolution in the increasingly distant past. Differences between geothermal and various proxy-based reconstructions have been ascribed mainly to different seasonal sensitivities in their temperature biases. For example tree ring proxies are sensitive to the growing season and ice core isotopes respond to the snow season. Proxies tend to be biased towards a particular season, whereas borehole temperatures respond to the surface temperature signal continuously and throughout the year.

Ground temperatures respond to surface air temperatures, but also to other processes that may superimpose non-climatic energy perturbations on the climatic signal. As discussed in ESM.1, a warmer season bias was implied in some studies, but the re-analysed data suggest that it contains both summer and winter effects, and additional data indicate that GST compares favorably to SAT trends even in the presence of snow and freeze/thaw cycles. Those results indicate air-ground coupling at decadal-to-centennial time scales and that geothermal reconstruction anomalies are robust long-term change indicators under conditions of conductive heat transport. Our reconstructed ground surface anomalies are thus interpreted to reflect SAT trends with the potential exception of the most recent decade, which might be affected by interannual variation in the offset between air and ground temperatures. The fact that both sites' histories are reminiscent of paleotemperature records suggests that the transferability to SAT is likely high, and that the differences between reconstructed temperature histories for the two sites most likely result from differences in meteorological conditions.

In the perennially frozen Arctic region, non-conductive processes affect the active layer. The reconstructed temperature histories represent the ground temperature changes at the upper boundary of the heat conduction domain [56], which, in this permafrost setting, is the top of permafrost. Even in the active layer, however, heat conduction is found to be the dominant process, with non-conductive transport contributing less than 3% to the mean heat flux [94]. Their results indicate that heat conduction plus a process description of freeze/thaw is appropriate to explain the thermal regime in the active layer. To assess the impact that latent heat effects may have on deeper permafrost temperatures, we modelled the reconstructed temperature history with the superposition of a seasonal freeze/thaw cycle. The result (Fig. S3 b) shows that latent heat effects have only a small impact on the recovered temperature history (see ESM.7 for more details).

The assumption of the initial subsurface temperature condition may bias our results. The equal levels of reconstructed surface temperature in the past at both sites, despite the observed colder deep permafrost temperatures at Mamontov Klyk, could also indicate that the initial conditions constructed from the deep Tiksi borehole were less appropriate for the Mamontov Klyk site. Mamontov Klyk is three times as far away from Tiksi as Sardakh, and its unconsolidated and relatively ice-rich subsurface differs in thermal diffusivity from the rocky Tiksi and Sardakh borehole sites, leading to potentially slower propagation of the Holocene transient warming signal. The Mamontov Klyk borehole is not deep enough to observe the geothermal gradient and the ambient quasi-steady-state temperature profile at the site. There are no other borehole data that could be used to evaluate the disparity between Tiksi and Mamontov Klyk. Nonetheless, transient Holocene warming is clearly visible in the borehole temperature record from Tiksi, indicating pre-warmed and not equilibrium conditions at the start of the reconstruction. We consider the effect of equilibrium initial conditions in ESM.6.

While the character of the specific inversion methods is reflected in the respective solutions as expected, a shortcoming in the resolving ability of the parameterization of the temperature history has a large impact on the reconstructed solution (ESM.8). The four-segment parameterization is only adequate to resolve the variations necessary in our reconstruction when used over a shorter time span of 150 a (Fig. S3 c). This shows that the choice of search space parameterization in optimization studies can be of high impact and must, therefore, be well considered. Nonetheless, the inversion solution of all three methods—when this limitation is taken into account—agrees quite well with each other. The reconstructed temperature histories thus seem robust against variation of the chosen inversion method.

Implications

Borehole temperature reconstructions from shallow permafrost boreholes prove successful in filling the gap of recent (up to the previous 200–300 a), well-resolved temperature records in the absence of tree ring proxies in the arctic tundra region. Resolution on the short time scale is good which overcomes poor age control in long-term radiometric dating techniques in this regard. For the Mamontov Klyk region, where no closer direct observations exist, this is the first time that a temperature record is recovered at this site of ongoing permafrost degradation. The reconstructed ground surface temperatures are directly valuable to permafrost models and to evaluating permafrost processes in the Siberian Arctic as they provide the temporal temperature changes at the permafrost table (the top of the mostly conductive regime) or at the standard depth of permafrost temperature observation (20 m below surface). The former parameter is the necessary upper boundary condition for forcing model assessments of the evolution of permafrost.

We caution that, due to the increasingly limited temporal resolution further back into the past, these reconstructions do not provide a means of comparing amplitudes of temperature change in recent time intervals to

those in intervals further in the past. Peaks here can be interpreted as a lower bound of temperature extrema. The uncertainty in the PSO solution distribution is a measure of the potential for short-term variation that is smoothed out by the diffusive processes. High frequencies are better resolved the more recent they are. As a consequence, the most current time span is the one with most detail. Nonetheless, the rapid recent increase is observed at both sites. Whether this signal will endure over longer time scales or remain transient (and be consequently smoothed out in future geothermal records as past transient high excursions may have today), will only become evident if the higher temperature persists in the future or by improving the resolution of the recovered temperature history. Combining the borehole temperature reconstructions with a proxy record with sensitivity to higher frequency modulations in the past of the temperature history could improve the resolution [20]. Unfortunately, even oxygen isotope variations in ice wedges do not achieve the required decadal resolution [62, 69].

Implications for the Laptev Sea region include:

(1) The reconstructed magnitude of changes is consistent with the observation that the region is amplified in its temperature changes even above the mean Arctic temperature change. This observation from the Tiksi SAT record is also in line with a recently reported c. 2.5 times higher warming rate for central Yakutia [8].
(2) The spatial differences between the two sites imply that climate trends did not necessarily affect both sites in the same way. This suggests that regional-scale temperature reconstructions are not necessarily valid locally.
(3) Despite the spatial variability, temperature histories at both sites are consistent with a recent rapid warming. This indicates that the recent warming signal is of synoptic scale and dominates over previous spatial variability.
(4) Our reconstructions provide information on the differences in the temperature history from simply using a shifted regional Arctic or even global mean temperature curve for the entire region. Studies of subsea permafrost distribution in the Russian Arctic [66, 79, 80] for example so far have utilized a global temperature trend curve adapted by offset for different locations due to the large-scale nature and the sparsity of data. However, our findings of spatial differences in the temperature trend during the last 200–300 a are a strong indicator that differences were probably present in earlier times, as well. Due to the spatial variability in the Laptev Sea region, site assessment of permafrost degradation might be strongly a priori biased if a larger scale mean temperature history instead of these local reconstructions is used.

Conclusions

Ground surface temperature histories reconstructed from borehole temperatures at two sites in the Laptev Sea region in the Russian Arctic show rapid recent warming. Local records of paleotemperature are sparse for this region, which is underrepresented in circum-Arctic temperature reconstructions. We used two inversion methods to find the most likely temperature histories required to describe the observed temperature profiles in the boreholes. Local differences, such as later warming and warming of higher magnitude, from current circum-Arctic temperature reconstructions were shown to exist in the study region. Spatial differences in past temperature trends between both sites suggest that additional records will uncover local-to-regional-scale variability. Understanding this spatial variability will depend on data on the variability of potential influences such as sea ice and snow cover. Our results provide a basis for local surface temperature record parameterization of climate models and permafrost models in particular.

Acknowledgements This work was partially funded by a Helmholtz Association Joint Russian-German Research Group (HGF JRG-100). The authors thank Frank Günther, Stefan Kruse, and Heidrun Matthes for assisting in data compilation; Tomas Opel and Volker Rath for helpful comments; and two anonymous reviewers for detailed comments and suggestions.

Compliance with ethical standard

Conflict of interest On behalf of all authors, the corresponding author states that there is no conflict of interest.

References

1. Andreev A, Tarasov P, Schwamborn G, Ilyashuk B, Ilyashuk E, Bobrov A, Klimanov V, Rachold V, Hubberten HW (2004) Holocene paleoenvironmental records from Nikolay Lake, Lena River Delta, Arctic Russia. Palaeogeogr Palaeoclimatol Palaeoecol 209:197–217. https://doi.org/10.1016/j.palaeo.2004.02.010
2. Andreev AA, Schirrmeister L, Tarasov PE, Ganopolski A, Brovkin V, Siegert C, Wetterich S, Hubberten HW (2011) Vegetation and climate history in the Laptev Sea region (Arctic Siberia) during Late Quaternary inferred from pollen records. Quat Sci Rev 30:2182–2199. https://doi.org/10.1016/j.quascirev.2010.12.026
3. Are F, Reimnitz E (2000) An overview of the Lena River delta setting: geology, tectonics, geomorphology, and hydrology. J Coast Res 16(4):1083–1093
4. Atlas Arktiki (1985) GUGK, Moscow (**in Russian**)
5. Bauch H, Mueller-Lupp T, Taldenkova E, Spielhagen R, Kassens H, Grootes P, Thiede J, Heinemeier J, Petryashov V (2001) Chronology of the Holocene transgression at the North Siberian margin. Global Planet Chang 31:125–139. https://doi.org/10.1016/S0921-8181(01)00116-3

6. Beltrami H, Ferguson G, Harris RN (2005) Long-term tracking of climate change by underground temperatures. Geophys Res Lett 32(19):L19707. https://doi.org/10.1029/2005GL023714
7. Boike J, Kattenstroth B, Abramova K, Bornemann N, Chetverova A, Fedorova I, Fröb K, Grigoriev M, Grüber M, Kutzbach L, Langer M, Minke M, Muster S, Piel K, Pfeiffer EM, Stoof G, Westermann S, Wischnewski K, Wille C, Hubberten HW (2013) Baseline characteristics of climate, permafrost and land cover from a new permafrost observatory in the Lena River Delta, Siberia (1998–2011). Biogeosciences 10(3):2105–2128. https://doi.org/10.5194/bg-10-2105-2013
8. Boike J, Grau T, Heim B, Günther F, Langer M, Muster S, Gouttevin I, Lange S (2016) Satellite-derived changes in the permafrost landscape of central Yakutia, 2000–2011: wetting, drying, and fires. Global Planet Chang 139:116–127. https://doi.org/10.1016/j.gloplacha.2016.01.001
9. Briffa KR, Osborn TJ, Schweingruber FH, Harris IC, Jones PD, Shiyatov SG, Vaganov EA (2001) Low-frequency temperature variations from a northern tree ring density network. J Geophys Res 106(D3):2929–2941. https://doi.org/10.1029/2000JD900617
10. Brown RD, Brasnett B (2015) Canadian Meteorological Centre (CMC) Daily snow depth analysis data. Environment Canada, 2010. Boulder, Colorado USA: National Snow and Ice Data Center. https://nsidc.org/data/docs/daac/nsidc0447_CMC_snow_depth/ **(updated annually)**. Accessed 2017
11. Bulygina ON, Razuvaev VN (2012) Daily Temperature and precipitation data for 518 Russian Meteorological Stations. Technical report, carbon dioxide information analysis center, Oak Ridge National Laboratory, U.S. Department of Energy, Oak Ridge, Tennessee. https://doi.org/10.3334/CDIAC/cli.100
12. Carson CJ, McLaren S, Roberts JL, Boger SD, Blankenship DD (2014) Hot rocks in a cold place: high sub-glacial heat flow in East Antarctica. J Geol Soc 171(1):9–12. https://doi.org/10.1144/jgs2013-030
13. CAVM Team (2003) Circumpolar Arctic Vegetation Map (1:7,500,000 scale). Conservation of Arctic flora and fauna (CAFF) Map No. 1. U.S. Fish and Wildlife Service, Anchorage, Alaska. http://www.geobotany.uaf.edu/cavm/finalcavm/index.html. Accessed 2016
14. Chapman DS, Bartlett MG, Harris RN (2004) Comment on "Ground vs. surface air temperature trends: Implications for borehole surface temperature reconstructions" by M. E. Mann and G. Schmidt. Geophys Res Lett 31(7):L07205. https://doi.org/10.1029/2003GL019054
15. Clow GD (1992) The extent of temporal smearing in surface-temperature histories derived from borehole temperature measurements. Global Planet Chang 6:81–86. https://doi.org/10.1016/0921-8181(92)90027-8
16. Crowley TJ (2000) Causes of climate change over the past 1000 years. Science 289(5477):270–277. https://doi.org/10.1126/science.289.5477.270
17. Davies JH (2013) Global map of solid Earth surface heat flow. Geochem Geophys Geosyst 14:4608–4622. https://doi.org/10.1002/ggge.20271
18. Demezhko DY, Gornostaeva AA (2015) Late Pleistocene-Holocene ground surface heat flux changes reconstructed from borehole temperature data (the Urals, Russia). Clim Past 11(4):647–652. https://doi.org/10.5194/cp-11-647-2015
19. Demezhko DY, Shchapov VA (2001) 80,000 years ground surface temperature history inferred from the temperature-depth log measured in the superdeep hole SG-4 (the Urals, Russia). Global Planet Chang 29:219–230. https://doi.org/10.1016/S0921-8181(01)00091-1
20. Demezhko DY, Solomina ON (2009) Ground surface temperature variations on Kunashir Island in the last 400 years inferred from borehole temperature data and tree-ring records. Dokl Earth Sci 426(1):628–631. https://doi.org/10.1134/S1028334X09040266
21. Ebbesen S, Kiwitz P, Guzzella L (2012) A generic particle swarm optimization Matlab function. Am Control Conf 2012:1519–1524
22. Ehlers J, Gibbard PL (2003) Extent and chronology of glaciations. Quat Sci Rev 22(15–17):1561–1568. https://doi.org/10.1016/S0277-3791(03)00130-6
23. Esper J, Cook ER, Schweingruber FH (2002) Low-frequency signals in long tree-ring chronologies for reconstructing past temperature variability. Science 295(5563):2250–2253. https://doi.org/10.1126/science.1066208
24. Galabala RO (1987) New data on the structure of the Lena Delta. In: Pokhialianen VP (ed) Quaternary Period Northeast Asia. SVKNII DVO AN SSSR, Magadan, pp 152–171 (**in Russian**)
25. Grakhanov S, Prokopiev A, Grakhanov O, Tarabukin V, Soloviev E (2013) New data on the geology of the Lena River delta area and the diamond potential of the Arctic region (in Russian). Fatherl Geol 5:33–40
26. Grigoriev M (1993) Cryomorphogenesis of the Lena River mouth area. Permafrost Institute Press SB RAS, Yakutsk (in Russian)
27. Grigoriev M, Imaev V, Imaeva L, Kozmin B, Kunitsky V, Larionov A, Mikulenko K, Skryabin R, Timirshin K (1996) Geology, seismicity, and cryogenic processes in the Arctic areas of western Yakutia (in Russian). Yakutian Scientific Center SD RAS, Yakutsk
28. Grigoriev MN, Rachold V (2003) The degradation of coastal permafrost and the organic carbon balance of the Laptev and East Siberian seas Permafrost. In: Proceedings of the 8th international conference on permafrost, 21–25 July 2003, Zurich, Switzerland, Balkema, Lisse, The Netherlands, pp 319–324
29. Grigoriev NF (1966) Mnogoletnemerzlyye porody primorskoy zony Yakutii (The permafrost of the coastal zone of Yakutia, in Russian). Nauka, Moscow
30. Grosse G, Schirrmeister L, Malthus TJ (2006) Application of Landsat-7 satellite data and a DEM for the quantification of thermokarst-affected terrain types in the periglacial Lena-Anabar coastal lowland. Polar Res 25(1):51–67. https://doi.org/10.1111/j.1751-8369.2006.tb00150.x/full
31. Grosse G, Robinson J, Bryant R, Taylor M, Harper W, DeMasi A, Kyker-Snowman E, Veremeeva A, Schirrmeister L, Harden J (2013) Distribution of late Pleistocene ice-rich syngenetic permafrost of the Yedoma Suite in east and central Siberia, Russia. Technical report, U.S. Geological Survey Open File Report 2013-1078
32. Günther F, Overduin PP, Yakshina IA, Opel T, Baranskaya AV, Grigoriev MN (2015) Observing Muostakh disappear: permafrost thaw subsidence and erosion of a ground-ice-rich island in response to arctic summer warming and sea ice reduction. Cryosphere 9(1):151–178. https://doi.org/10.5194/tc-9-151-2015
33. Hansen J, Ruedy R, Sato M, Lo K (2010) Global surface temperature change. Rev Geophys 48(4):RG4004. https://doi.org/10.1029/2010RG000345
34. Harris I, Jones P, Osborn T, Lister D (2014) Updated high-resolution grids of monthly climatic observations–the CRU TS3.10 Dataset. Int J Climatol 34(3):623–642. https://doi.org/10.1002/joc.3711
35. Harris RN, Chapman DS (2001) Mid-latitude (30° – 60° N) climatic warming inferred by combining borehole temperatures with surface air temperatures. Geophys Res Lett 28(5):747–750. https://doi.org/10.1029/2000GL012348
36. Ho SL, Laepple T (2016) Flat meridional temperature gradient in the early Eocene in the subsurface rather than surface ocean. Nat Geosci 9(8):606–610. https://doi.org/10.1038/ngeo2763
37. Huang S (2004) Merging information from different resources for new insights into climate change in the past and future. Geophys Res Lett 31(13):L13205. https://doi.org/10.1029/2004GL019781

38. Huang S, Pollack HN, Shen PY (2000) Temperature trends over the past five centuries reconstructed from borehole temperatures. Nature 403(6771):756–758. https://doi.org/10.1038/35001556
39. Huang SP, Pollack HN, Shen PY (2008) A late Quaternary climate reconstruction based on borehole heat flux data, borehole temperature data, and the instrumental record. Geophys Res Lett 35(13):L13703. https://doi.org/10.1029/2008GL034187
40. Ingebritsen SE, Sanford WE, Neuzil CE (2007) Groundwater in geologic processes. Cambridge University Press, Cambridge
41. International Heat Flow Commission (IHFC) (2011) The global heat flow database. http://www.heatflow.und.edu/. Accessed 2017
42. Ippisch O (2001) Coupled transport in natural porous media. PhD thesis, University of Heidelberg
43. Isaksen K, Benestad RE, Harris C, Sollid JL (2007) Recent extreme near-surface permafrost temperatures on Svalbard in relation to future climate scenarios. Geophys Res Lett 34(17):L17502. https://doi.org/10.1029/2007GL031002
44. Jaume-Santero F, Pickler C, Beltrami H, Mareschal JC (2016) North American regional climate reconstruction from ground surface temperature histories. Clim Past 12(12):2181–2194. https://doi.org/10.5194/cp-12-2181-2016
45. Jones PD, Mann ME (2004) Climate over past millennia. Rev Geophys 42(2):RG2002. https://doi.org/10.1029/2003RG000143
46. Jones PD, Lister DH, Osborn TJ, Harpham C, Salmon M, Morice CP (2012) Hemispheric and large-scale land-surface air temperature variations: an extensive revision and an update to 2010. J Geophys Res 117(D5):D05127. https://doi.org/10.1029/2011JD017139
47. Jouzel J, Masson-Delmotte V, Cattani O, Dreyfus G, Falourd S, Hoffmann G, Minster B, Nouet J, Barnola JM, Chappellaz J, Fischer H, Gallet JC, Johnsen S, Leuenberger M, Loulergue L, Luethi D, Oerter H, Parrenin F, Raisbeck G, Raynaud D, Schilt A, Schwander J, Selmo E, Souchez R, Spahni R, Stauffer B, Steffensen JP, Stenni B, Stocker TF, Tison JL, Werner M, Wolff EW (2007) Orbital and millennial antarctic climate variability over the past 800,000 years. Science 317(5839):793–796. https://doi.org/10.1126/science.1141038
48. Kogan A (1974) The setting of seismic works using the method KMPV-GSZ from sea ice on the shelf of the Arctic Seas (in Russian). Geophys Methods Explor Arctic 9:33–38 (L:NIIGA)
49. Kurek J, Cwynar LC, Ager TA, Abbott MB, Edwards ME (2009) Late Quaternary paleoclimate of western Alaska inferred from fossil chironomids and its relation to vegetation histories. Quat Sci Rev 28(9):799–811. https://doi.org/10.1016/j.quascirev.2008.12.001
50. Lachenbruch A, Marshall B (1986) Changing climate: geothermal evidence from permafrost in the Alaskan Arctic. Science 234(4777):689–696. https://doi.org/10.1126/science.234.4777.689
51. Langer M, Westermann S, Muster S, Piel K, Boike J (2011) The surface energy balance of a polygonal tundra site in northern Siberia-Part 2: winter. Cryosphere 5(2):509–524. https://doi.org/10.5194/tc-5-509-2011
52. Langer M, Westermann S, Heikenfeld M, Dorn W, Boike J (2013) Satellite-based modeling of permafrost temperatures in a tundra lowland landscape. Remote Sens Environ 135:12–24. https://doi.org/10.1016/j.rse.2013.03.011
53. Lawrence DM, Slater AG, Tomas RA, Holland MM, Deser C (2008) Accelerated Arctic land warming and permafrost degradation during rapid sea ice loss. Geophys Res Lett 35(11):L11506. https://doi.org/10.1029/2008GL033985
54. Lawrimore JH, Menne MJ, Gleason BE, Williams CN, Wuertz DB, Vose RS, Rennie J (2011) An overview of the Global Historical Climatology Network monthly mean temperature data set, version 3. J Geophys Res Atmos 116(D19):D19121. https://doi.org/10.1029/2011JD016187
55. Ljungqvist FC (2010) A new reconstruction of temperature variability in the extra-tropical Northern Hemisphere during the last two millennia. Geogr Ann Ser A Phys Geogr 92(3):339–351
56. Majorowicz J, Safanda J, Skinner W (2004) Past surface temperature changes as derived from continental temperature logs—Canadian and some global examples of application of a new tool in climate change studies. Adv Geophys 47:113–174. https://doi.org/10.1016/S0065-2687(04)47003-4 (Elsevier)
57. Mann ME, Bradley RS, Hughes MK (1999) Northern hemisphere temperatures during the past millennium: inferences, uncertainties, and limitations. Geophys Res Lett 26(6):759–762. https://doi.org/10.1029/1999GL900070
58. Mann ME, Zhang Z, Hughes MK, Bradley RS, Miller SK, Rutherford S, Ni F (2008) Proxy-based reconstructions of hemispheric and global surface temperature variations over the past two millennia. Proc Natl Acad Sci 105(36):13252–13257. https://doi.org/10.1073/pnas.0805721105
59. Marcott SA, Shakun JD, Clark PU, Mix AC (2013) A reconstruction of regional and global temperature for the past 11,300 years. Science 339(6124):1198–1201. https://doi.org/10.1126/science.1228026
60. McGuire AD, Anderson LG, Christensen T, Dallimore S, Guo L, Hayes DJ, Heimann M, Lorenson TD, Macdonald RW, Roulet N (2009) Sensitivity of the carbon cycle in the Arctic to climate change. Ecol Monogr 79:523–555. https://doi.org/10.1890/08-2025.1
61. McKay NP, Kaufman DS (2014) An extended Arctic proxy temperature database for the past 2,000 years. Sci Data 1(140):026. https://doi.org/10.1038/sdata.2014.26
62. Meyer H, Opel T, Laepple T, Dereviagin AY, Hoffmann K, Werner M (2015) Long-term winter warming trend in the Siberian Arctic during the mid- to late Holocene. Nat Geosci 8(2):122–125. https://doi.org/10.1038/ngeo2349
63. Moberg A, Sonechkin DM, Holmgren K, Datsenko NM, Karlen W (2005) Highly variable Northern Hemisphere temperatures reconstructed from low- and high-resolution proxy data. Nature 433(7026):613–617. https://doi.org/10.1038/nature03265
64. Mueller K (1997) Oberflächenstrukturen und Eigenschaften von Permafrostböden im nordsibirischen Lena-Delta (in German). Z Pflanzenernaehr Bodenk 160(4):497–503. https://doi.org/10.1002/jpln.19971600410
65. National Climatic Data Center, NOAA (2015) Climate data online, station Tiksi. https://www.ncdc.noaa.gov/cdo-web/datasets/GHCND/stations/GHCND:RSM00021824/detail. Accessed 2015
66. Nicolsky DJ, Romanovsky VE, Romanovskii NN, Kholodov AL, Shakhova NE, Semiletov IP (2012) Modeling sub-sea permafrost in the East Siberian Arctic Shelf: the Laptev Sea region. J Geophys Res Earth Surf 117(F03):028. https://doi.org/10.1029/2012JF002358
67. Oerlemans J (2005) Extracting a climate signal from 169 glacier records. Science 308(5722):675–677. https://doi.org/10.1126/science.1107046
68. Opel T, Fritzsche D, Meyer H (2013) Eurasian Arctic climate over the past millennium as recorded in the Akademii Nauk ice core (Severnaya Zemlya). Clim Past 9(5):2379–2389. https://doi.org/10.5194/cp-9-2379-2013
69. Opel T, Laepple T, Meyer H, Dereviagin AY, Wetterich S (2017) Northeast Siberian ice wedges confirm Arctic winter warming over the past two millennia. Holocene. https://doi.org/10.1177/0959683617702229
70. Orsi AJ, Cornuelle BD, Severinghaus JP (2012) Little ice age cold interval in West Antarctica: evidence from borehole temperature at the West Antarctic ice sheet (WAIS) divide. Geophys Res Lett 39(9):L09710. https://doi.org/10.1029/2012GL051260

71. Overduin P, Grigoriev M, Junker R, Rachold V, Kunitsky V, Bolshiyanov D, Schirrmeister L (2007) The expedition COAST I: COAST drilling campaign 2005: subsea permafrost studies in the near-shore zone of the Laptev Sea. Rep Polar Res 550:1–40
72. PAGES 2k Consortium (2013) Continental-scale temperature variability during the past two millennia. Nat Geosci 6(5):339–346. https://doi.org/10.1038/ngeo1797
73. Peterson BJ, Holmes RM, McClelland JW, Vörösmarty CJ, Lammers RB, Shiklomanov AI, Shiklomanov IA, Rahmstorf S (2002) Increasing river discharge to the Arctic Ocean. Science 298(5601):2171–2173. https://doi.org/10.1126/science.1077445, http://science.sciencemag.org/content/298/5601/2171.full.pdf
74. Pollack HN, Smerdon JE (2004) Borehole climate reconstructions: spatial structure and hemispheric averages. J Geophys Res 109(D11):D11106. https://doi.org/10.1029/2003JD004163
75. Pollack HN, Hurter SJ, Johnson JR (1993) Heat flow from the Earth's interior: analysis of the global data set. Rev Geophys 31(3):267–280. https://doi.org/10.1029/93RG01249
76. Pollack HN, Demezhko DY, Duchkov AD, Golovanova IV, Huang S, Shchapov VA, Smerdon JE (2003) Surface temperature trends in Russia over the past five centuries reconstructed from borehole temperatures. J Geophys Res 108(B4):2180. https://doi.org/10.1029/2002JB002154
77. Reliable Prognostics (2017) Weather archive on Stolb Island. https://rp5.ru/Weather_archive_on_Stolb_Island. Accessed 23 Feb 2017
78. Roberts JL, Moy AD, van Ommen TD, Curran MAJ, Worby AP, Goodwin ID, Inoue M (2013) Borehole temperatures reveal a changed energy budget at Mill Island, East Antarctica, over recent decades. Cryosphere 7(1):263–273. https://doi.org/10.5194/tc-7-263-2013
79. Romanovskii N, Hubberten H, Romanovsky V, Kholodov A (2003) Permafrost evolution under the influence of long-term climate fluctuations and glacio-eustatic sea-level variation: region of Laptev and East Siberian Seas, Russia. In: Phillips M, Springman SM, Arenson LU (eds) Permafrost: proceedings of the 8th international conference on permafrost, 21–25 July 2003, Zurich, Switzerland, Balkema, vol 2, pp 983–987
80. Romanovskii N, Hubberten H, Gavrilov A, Tumskoy V, Kholodov A (2004) Permafrost of the east Siberian Arctic shelf and coastal lowlands. Quat Sci Rev 23(11–13):1359–1369. https://doi.org/10.1016/j.quascirev.2003.12.014
81. Schirrmeister L, Grosse G, Kunitsky V, Magens D, Meyer H, Dereviagin A, Kuznetsova T, Andreev A, Babiy O, Kienast F, Grigoriev M, Overduin PP, Preusser F (2008) Periglacial landscape evolution and environmental changes of Arctic lowland areas for the last 60,000 years (western Laptev Sea coast, Cape Mamontov Klyk). Polar Res 27(2):249–272. https://doi.org/10.1111/j.1751-8369.2008.00067.x
82. Schirrmeister L, Kunitsky V, Grosse G, Wetterich S, Meyer H, Schwamborn G, Babiy O, Derevyagin A, Siegert C (2011) Sedimentary characteristics and origin of the Late Pleistocene ice complex on north-east Siberian Arctic coastal lowlands and islands—a review. Quat Int 241(1–2):3–25. https://doi.org/10.1016/j.quaint.2010.04.004
83. Schirrmeister L, Froese D, Tumskoy V, Grosse G, Wetterich S (2013) Yedoma: Late Pleistocene ice-rich syngenetic permafrost of Beringia. In: Elias SA (ed) The encyclopedia of quaternary science, vol 3. Elsevier, Amsterdam, pp 542–552
84. Schuur EAG, Vogel JG, Crummer KG, Lee H, Sickman JO, Osterkamp TE (2009) The effect of permafrost thaw on old carbon release and net carbon exchange from tundra. Nature 459(7246):556–559. https://doi.org/10.1038/nature08031
85. Schwamborn G, Rachold V, Grigoriev MN (2002) Late Quaternary sedimentation history of the Lena Delta. Quat Int 89(1):119–134. https://doi.org/10.1016/S1040-6182(01)00084-2
86. Schwamborn GJ (2004) Late quaternary sedimentation history of the Lena delta = Spätquartäre Sedimentationsgeschichte im Lena-Delta, Berichte zur Polar- und Meeresforschung (Reports on Polar and Marine Research), vol 471. Alfred Wegener Institute for Polar and Marine Research, Bremerhaven, Germany
87. Shi F, Yang B, Mairesse A, von Gunten L, Li J, Bräuning A, Yang F, Xiao X (2013) Northern Hemisphere temperature reconstruction during the last millennium using multiple annual proxies. Clim Res 56(3):231–244. https://doi.org/10.3354/cr01156
88. Smerdon JE, Stieglitz M (2006) Simulating heat transport of harmonic temperature signals in the Earth's shallow subsurface: lower-boundary sensitivities. Geophys Res Lett 33(14):L14402. https://doi.org/10.1029/2006GL026816
89. Stevens MB, Smerdon JE, Gonzalez-Rouco JF, Stieglitz M, Beltrami H (2007) Effects of bottom boundary placement on subsurface heat storage: implications for climate model simulations. Geophys Res Lett 34(2):L02702. https://doi.org/10.1029/2006GL028546
90. Timokhov L (1994) Regional characteristics of the Laptev and the East Siberian Seas: Climate, topography, ice phases, thermohaline regime, circulation. In: Kassens H, Hubberten HW, Pryamikov SM, Stein R (eds) Russian–German Cooperation in the Siberian Shelf Seas: geo-system Laptev-Sea. Ber, Polarforsch, p 144
91. Vavrus S, Holland MM, Bailey DA (2011) Changes in Arctic clouds during intervals of rapid sea ice loss. Clim Dyn 36(7):1475–1489. https://doi.org/10.1007/s00382-010-0816-0
92. de Vries D (1963) The thermal properties of soils. In: van Wijk R (ed) Physics of plant environment. North Holland, Amsterdam, pp 210–235
93. Wagner D, Kobabe S, Pfeiffer EM, Hubberten HW (2003) Microbial controls on methane fluxes from a polygonal tundra of the Lena Delta, Siberia. Permafrost Periglac Process 14(2):173–185. https://doi.org/10.1002/ppp.443
94. Weismüller J, Wollschläger U, Boike J, Pan X, Yu Q, Roth K (2011) Modeling the thermal dynamics of the active layer at two contrasting permafrost sites on Svalbard and on the Tibetan Plateau. Cryosphere 5(3):741–757. https://doi.org/10.5194/tc-5-741-2011
95. Winterfeld M, Schirrmeister L, Grigoriev MN, Kunitsky VV, Andreev A, Murray A, Overduin PP (2011) Coastal permafrost landscape development since the Late Pleistocene in the western Laptev Sea, Siberia. Boreas 40(4):697–713. https://doi.org/10.1111/j.1502-3885.2011.00203.x
96. Yang D, Liu B, Ye B (2005) Stream temperature changes over Lena River Basin in Siberia. Geophys Res Lett 32(5):L05401. https://doi.org/10.1029/2004GL021568
97. Overduin P, Rachold V, Grigoriev MN (2008) The state of subsea permafrost in the Western Laptev Nearshore zone. In: Proceedings of the 9th international conference on permafrost, Fairbanks, Alaska, pp 1345–1350